Colors of thermal pools at Yellowstone National Park

Paul W. Nugent,[1] Joseph A. Shaw,[1,*] and Michael Vollmer[2]

[1]Electrical and Computer Engineering Department, Montana State University, Bozeman, Montana 59717, USA

[2]Brandenburg University of Applied Sciences, Germany

*Corresponding author: jshaw@montana.edu

Received 1 October 2014; accepted 25 October 2014;
posted 24 November 2014 (Doc. ID 224271); published 19 December 2014

The brilliant visible colors of various hot springs and pools in Yellowstone National Park are explained with a combination of scattering from the water and from microbial mats that coat the bottoms of these thermal features. A simple 1D radiative transfer model was used to simulate the colors recorded in visible photographs and the spectrum of light making up these colors. The model includes attenuation in water by absorption and molecular scattering as well as reflection characteristics of the microbial mats and surface reflection of the water. Pool geometries are simulated as simple rough cones scaled to have depths and widths that match published data. Thermal images are also used to record the spatial distribution of water skin temperature. The measurements and simulations confirm that colors observed from shallow-water features arise primarily from the spectral properties of the microbial mat, which is related to the water temperature, while colors observed from deeper water arise primarily from the wavelength-dependent absorption and scattering in the water.

OCIS codes: (010.0010) Atmospheric and oceanic optics; (010.7340) Water; (010.1690) Color.
http://dx.doi.org/10.1364/AO.54.00B128

1. Introduction

The hot springs of Yellowstone National Park (YNP) greet visitors with a brilliant spectrum of colors, which often leave lasting impressions [1]. They are so visually striking that the 1871 Hayden Expedition report said: "…nothing ever conceived by human art could equal the peculiar vividness and delicacy of color of these remarkable prismatic springs" [2]. Individual basic mechanisms underlying the observed pool colors are well known in certain communities (e.g., microbial mat colors are well understood in the biology community and colors of pure water are well understood by the ocean optics community), but our aim in this paper is to summarize these mechanisms and explain the observed pool colors to the optics community using a combination of spectral reflectance measurements, photographs, thermal images, and simple radiative transfer simulations.

Today it is well known that the primary source of the beautiful colors of thermal pools and outflows are the microbial communities that thrive in these hot waters of temperature typically between 60°C and 70°C, and sometimes in excess of 90°C [3,4]. These communities often form optically thick mats of several mm thickness covering the rock wall of the pools, comprised of complex communities of thermophiles, primarily cyanobacteria but also other bacteria and archaea [5,6]. The understanding of the relationship between the colors of the microbial mats and different species within the microbial community has built on studies that suggested that the source may have been a nonliving form of mineral, possibly some bizarre form of silica [7] or, more correctly, the mats found in hot pools and outflows were biological in nature, possibly a form of algae [7,8]. It is now understood that these mats are comprised of complex communities of microbes, primarily thermophilic cyanobacteria (often called blue-green algae) and other thermophilic bacteria and archaea [5,6,9]. Such springs and their associated color-producing

1559-128X/15/04B128-12$15.00/0

cyanobacteria are found in diverse locations, including New Zealand [10,11], Japan [12], Iceland, Blood Falls in Antarctica, Indonesia, and—the focus of this paper—YNP in the United States [3,4,9].

The spectrum of colors present in shallow outflows is caused by photosynthetic pigments in different species of bacteria (and archaea) that thrive at different water temperatures in the pool [13]. Additional physicochemical factors, such as pH, sulfur content, and light intensity also play a significant role in the speciation and, hence, the colors of a particular pool [13,14]. Studies encompassing a broad range of hot springs have shown the predominant mat-forming bacteria to be cyanobacteria up to 74°C, communities of cyanobacteria and *chloroflexus* below 70°C, or cyanobacteria and *chromatiaceae* below 57°C [15,9]. The green, orange, brown, and yellow mats are evidence of photosynthesis in the predominately cyanobacteria communities [13]. The yellow and brown colors come from carotenoids and phycobiliproteins, which transfer energy to chlorophyll and provide indirect protection from high solar irradiance. These accessory pigments absorb from 400 to 500 nm, giving the mat a yellow or orange tint [13]. Within the neutral to slightly basic pools of YNP, photosynthesis has an upper limit of 75°C (this limit is lower in acidic pools) [13].

Although photosynthesis has a temperature limit, no pool or water source within YNP is truly sterile. Even the white-bottomed pools and streams with waters near boiling (~92°C at the high altitude of YNP) contain life [13]. As early as 1927, the presence of chlorophyll-lacking "algae" (likely bacteria or archaea) was noted in waters above 90°C [16]. These bacteria and archaea exist well above the limit of photosynthesis by relying on chemolithotrophic or heterotrophic processes [17]. In fact, the high temperature limit of life is well beyond the temperatures reached in the pools of YNP, as extreme thermophiles have been observed in the superheated water surrounding undersea geothermal vents up to 121°C [13]. Temperature is not the only determining factor, but it does play a strong role in the species diversity of the microbial communities [6]. In some cases, there can be a clear relationship between the colors of the microbial communities and temperature. This is illustrated in Table 1, which builds on Weed's early observation supplemented with new information about the type of microbes present [8,13,15,18].

The color patterns of a particular pool do not necessarily match those described in the tables, nor do the colors of YNP necessarily match the colors of other regions. For example, thermal pools near Nakabusa, Japan exhibit a different temperature-driven species change: green at 48°C, orange at 58°C, brown at 60°C, and white at 73°C. This is attributed to the role of geological isolation in the genetics of cyanobacteria and other thermophiles dispersed among pools; even within YNP, the genetic differences produce four distinct regions: (a) Mammoth, (b) Norris, (c) Upper/Middle/Lower Geyser Basins, and (d) the vicinity of Yellowstone Lake [11]. Seasonal changes in mat color have been observed, and include seasonal color fading, which has been shown to not relate to chemical changes in the pools and could be explained by changes in water temperature and UV–visible irradiance [18].

In addition to the microbial mats, a second influence on colors of pools—especially deeper pools—is optical absorption and scattering in the water, effectively the color of water. In these pools, the colors of the underlying microbial mat combine with wavelength-dependent absorption and scattering in the water [19,20] to significantly alter the observed pool colors as a function of pool depth. The color of water has been the topic of many detailed studies that include ocean colors [19,21,22] and pure laboratory water [20]. These studies have shown that water color is primarily affected by wavelength-selective absorption [19], and secondarily by wavelength-dependent scattering [20]. Scattering becomes increasingly important as the depth of clear pools or the water turbidity increases. For example, in deep water an absorption model alone would predict a pool with a dark nearly black center, the only light being due to reflections from the surface. However, the ever-present scattering can change the observed colors appreciably.

Whereas, ocean color is greatly impacted by absorption and scattering from chlorophyll, organic substances, and hydrosols with dimension <10 μm [21], the hot clear pools of geothermal areas often have temperatures too warm for chlorophyll-producing bacteria or algae, and therefore the organic substance is not expected. Nevertheless, optical scattering by suspended particulates can be a dominant color-producing mechanism in thermal pools. An example is the milky blue pools of the Beppu area

Table 1. Biological Colors and Associated Temperatures in YNP

Observed Color	Approximate Temperature (°C)	Microorganisms
Brown, red, green	43	Various algae, protozoa, bacteria
Orange	57	Cyanobacteria and *Chromatiaceae*
Yellow, Green, or greenish-yellow	70	Cyanobacteria and *Chloroflexus*
Yellow	75	Cyanobacteria
Limit to photosynthesis	75	
Pink	83	Chemolithotrophic or heterotrophic bacteria and archaea
White	85	Chemolithotrophic or heterotrophic bacteria and archaea

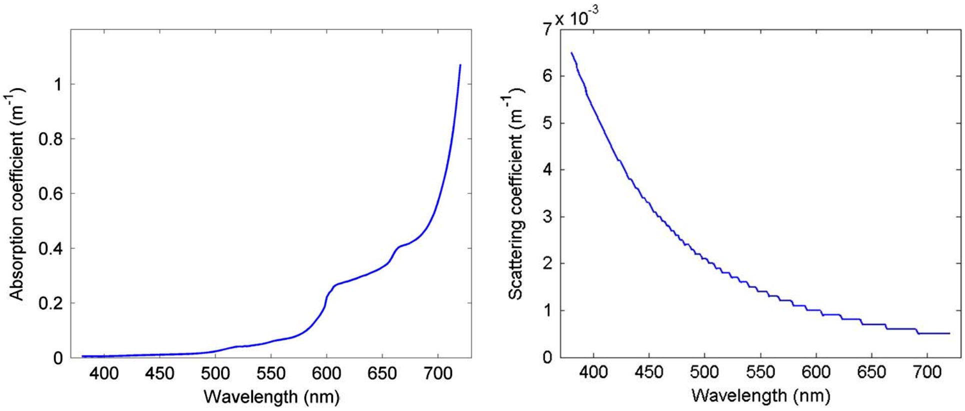

(a) (b)

Fig. 1. Pure water optical properties: (a) absorption coefficient α in m^{-1}; and (b) scattering coefficient b in m^{-1} [20].

in southwestern Japan. The color of these pools has been attributed to increased shortwave scattering owing to a suspension of subwavelength particles [12]. Similarly, cold water lakes with glacial inflows often have a very high amount of scattering particles that cause their characteristic turquoise or even gray color [23]. A suspension of particulates is likely the cause of the milky blue hue in some pools in YNP, such as Wall Pool, but it cannot explain the colors of clear-water pools, such as Grand Prismatic Spring, discussed in this paper. The main difference between the pools in these various studies is the water turbidity, with the clear-water pools having much reduced scattering and absorption that allow the observed colors to be appreciably affected by light reflected from the bottom material of the pool [24]. As a result, the colors of clear-water pools must be explained by a combination of the optical properties of clear natural water and the spectral reflectance of the bottom material.

Several recent studies have simulated observations from natural waters and lakes. For example, the brilliant blue, green, and greenish-yellow colors of Lake Onneto in Japan have been reproduced using a combination of inherent optical properties of water, color-producing agents in the lake, and yellowish bottom sediments, showing good comparison with spectroradiometric measurements [25].

In this paper, we take a similar approach for the water of YNP, but for simplicity we use temperature-dependent spectral absorption and scattering of pure water [20]. These water properties are used in a simple 1D radiative transfer model incorporating water absorption and scattering, atmospheric absorption and scattering, and illuminating solar radiation to reproduce the colors of Sapphire Pool, Morning Glory pool, and Grand Prismatic Spring in YNP. This model incorporates spectral reflectance measurements of the sky, microbial mats, water, and soil at various locations within and near the pools. Simulated images are compared with photographs and simulated spectra are compared with measured spectra. Thermal images are used to aid in interpretation of the observed color patterns in pools. The results are discussed in a manner to build an understanding of the optical principles leading to the colors of both shallow and deep-water pools.

2. Modeling Methodology

Pool colors were simulated using a 1D radiative transfer model that incorporated the water absorption coefficient a and scattering coefficient b (as shown in Fig. 1, [20]) to simulate the optical propagation through the water. The model also used spectral measurements of the microbial mat or rock reflectance, Fresnel reflectance at the top water surface, and an atmospheric model of the incident direct solar illumination and diffusely scattered skylight. The spectral reflectance of the microbial mats and soils were measured with a hand-held spectrometer (Ocean Optics USB4000) at various locations within and near the pools.

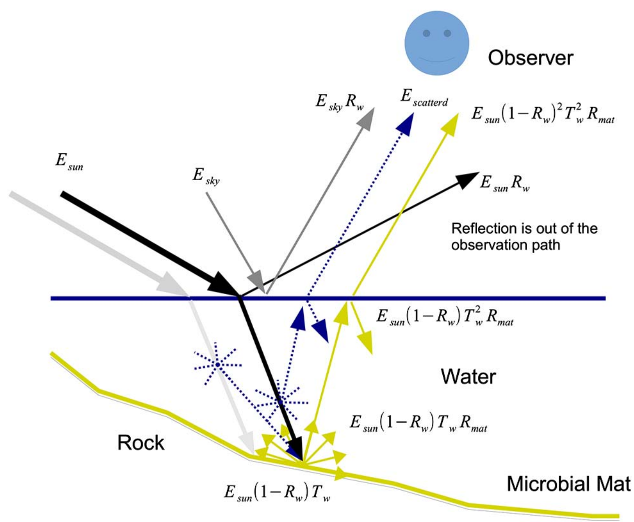

Fig. 2. Graphical depiction of the terms making up the model of observed upwelling spectral irradiance $E(\lambda)$: diffuse skylight spectral irradiance $E_{\mathrm{sky}}(\lambda)$ reflected from the water (gray arrow); solar spectral irradiance $E_{\mathrm{sun}}(\lambda)$ reflected from the bottom (yellow arrow); and sunlight scattered within the water (dashed blue arrow). For clarity of the description, only a few paths of the upwelling light are shown.

(a)

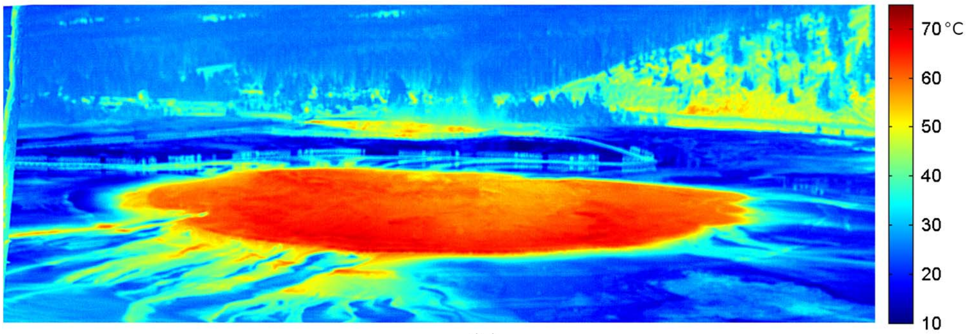

(b)

Fig. 3. (a) Photograph of Grand Prismatic Spring in YNP, showing the orange and yellow colors of the microbial mats in the shallow waters surrounding the pool and greens and blues in the deeper waters of the pool. (b) Thermal image of Grand Prismatic Spring using 8 stitched images from a FLIR Photon 640 infrared camera. The image displays low temperatures in blue and high temperatures in red.

A graphical overview of the modeling process is shown in Fig. 2 for an observation angle chosen to exclude specular solar reflection. The figure indicates the three primary components of the light seen by an observer or camera: diffuse skylight spectral irradiance $E_{\mathrm{sky}}(\lambda)$ reflected from the water (gray arrow), solar spectral irradiance diffusely reflected from the bottom (yellow arrow), and sunlight scattered within the water (dashed blue arrow). The total upward spectral irradiance $E(\lambda)$ seen by the observer is described by Eq. (1) using notation from the *Handbook of Optics* [26].

$$E(\lambda) = E_{\mathrm{sky}}(\lambda)R_w + E_{\mathrm{sun}}(\lambda)(1 - R_w)^2 R_{\mathrm{mat}} T_w^2 + E_{\mathrm{scattered}}(\lambda), \tag{1}$$

with

$$T_w^2(\lambda) = e^{-(a+\frac{b}{2})2z}, \tag{2}$$

and

$$E_{\mathrm{scattered}}(\lambda) = E_{\mathrm{sun}}(\lambda)(1 - R_w)^2 \sum_{n=0}^{z/\Delta l} e^{-2(a+\frac{b}{2})n\Delta z}(1 - e^{-\frac{b}{2}\Delta z}). \tag{3}$$

For the scheme shown in Fig. 2, Eq. (1) is a simplified 1D model used to describe the hemispheric-averaged upward irradiance from the pool in terms of the downward solar irradiance and diffuse skylight. Our observation angles were chosen to avoid specular reflection of sunlight from the water, and thus the model assumes the solar specular reflection $E_{\mathrm{sun}}R_w$ can be ignored. The relative magnitude of terms can be considered by noting that diffuse sky irradiance at the ground is approximately one order of magnitude smaller than direct solar irradiance for a clear sky.

The first term of the right-hand side of Eq. (1) (left reflected arrow in Fig. 2) is diffuse skylight spectral irradiance $E_{\mathrm{sky}}(\lambda)$ reflected from the water with Fresnel reflectance R_w. A polarized model of smooth-surface Fresnel reflection was used to model the water surface reflection at each observation angle, but the cameras were sufficiently insensitive to polarization so that the polarization terms were added.

The second term (right reflected arrow in Fig. 2) is solar spectral irradiance backward scattered from the mat with unpolarized spectral reflectance $R_{\mathrm{mat}}(\lambda)$, modified by double-pass attenuation in the water [Eq. (2)] with absorption coefficient a along a total path length in the water of $2z$. Here, z describes the downward and upward path lengths within the water which, for simplicity, were assumed to be equal. In our 1D model, the scattering contribution was described by $b/2$ rather than using the total scattering coefficient b because forward-scattered light contributes to the observed signal and only backscattering leads to attenuation. For simplicity, forward and backscattering were assumed to be equal and the scattering from the mat was assumed to be Lambertian (i.e., scattered radiance is independent of observation angle).

The third and last term (middle reflected arrow in Fig. 2) is sunlight scattered within the water [Eq. (3)]. This term describes a multilayer radiative transfer model in which Δz is the layer thickness (1 cm here). The model uses $b/2$ to approximate the scattering coefficient for light scattered into the backward or forward hemisphere. It is important to note that as the downward-propagating light is scattered, the forward-scattered light still contributes to the total illumination at the bottom of the pool. Similarly, as the upward-propagating light is scattered, the forward-scattered light contributes to the observed light. In Eq. (3) describing the scattered light, the first term in the sum $e^{-2(a+b/2)n\Delta z}$ describes the attenuation along the path between the water surface and the current layer and the factor 2 accounts for upward propagation back toward the surface along a path of equal length. The second term $(1 - e^{-(b/2)\Delta z})$ describes the scattering within each layer. The summation over all layers down to the depth of the mat gives the total upward-scattered light that may be observed above the water surface. The summation of these three terms gives the total backward-scattered light seen by an observer looking into the pool.

The spectra of diffuse skylight and direct solar irradiance were modeled with MODTRAN5 [27], using temperature and humidity profiles determined by scaling the 1976 Standard Atmosphere [28] so that the surface atmospheric layer matched meteorological data from the US SNOTEL station 384 at Canyon, WY [29]. The pressure profile of the 1976 Standard Atmosphere was adjusted for the elevation of each pool. All other absorbing gases were modeled with the 1976 Standard Atmosphere default values, except the CO_2 mixing ratio was increased to 393 ppm to match the Mauna Loa Observatory measurement for that time [30].

We note that, on the days of our measurements (see below), there was a notable amount of smoke in the air, which led to somewhat blue-depleted skylight reflecting from the water surfaces. The closest source of aerosol data is our solar radiometer located in Bozeman, Montana, approximately 130 km from the Yellowstone pools. It recorded an average aerosol optical depth of 0.70 on 8 Aug. 2012 and 0.44 on 23 Aug. 2012 (for 500-nm wavelength), both much higher than the clean-air values that are typically much less than 0.1. Since exact values for our measurement locations were not known, we did not include increased aerosol attenuation in the model, but this may account for some residual color differences.

Because we did not have detailed pool bathymetry data, we simulated cone-shaped pools scaled to have depths and widths that match published data [3,4]. A fractal noise pattern was added to the circular cone ends to approximate a natural pool outline and add texture to the pool [31]. The cooler pools were simulated with a bottom surface spectral reflectance measured for the mats found in the warmest shallow waters near the pool. The hottest pools, such as Sapphire Pool, were simulated without a microbial mat, using the spectral reflectance of the bare rock at the edge of the pool.

The pool color modeling procedure incorporated the following steps.

1. Determine the microbial mat properties using published pool temperatures [3,4] and shallow water spectra of nearby microbial mats.
2. Use published shapes and depths [3,4] to create an approximate 3D geometric model of the pool.
3. Determine solar angle from time of day, latitude, and longitude.
4. Run a MODTRAN model to determine solar spectral irradiance of sunlight $E_{\mathrm{sun}}(\lambda)$ and diffuse skylight at the water surface $E_{\mathrm{sky}}(\lambda)$.
5. Use the viewing angle to calculate the water reflectance R_w and observation path length.
6. Simulate spectra for all depths using Eq. (1) for all pixels in the pool scene.
7. Pass each pixel's spectrum through an RGB CMOS camera model, with red, green, and blue spectral responses for a Bayer-pattern silicon detector and apply a white balance adjusted for sunlight.

3. Yellowstone Measurements and Simulations

On 8 and 23 August 2012, measurements were taken in YNP using digital SLR cameras for visible images, long wave infrared (LWIR) thermal imaging cameras (FLIR Photon 640 and FLIR Photon 320) for noncontact measurement of water temperatures, and a portable optical spectrometer (Ocean Optics USB4000, 350—1000 nm) to measure the spectral reflectance of the microbial mats, soil, and water. These measurements were entirely passive, only using the natural light or thermal radiation emitted from the pools. The following section describes the measurements and simulation results for some specific pools in YNP. It includes spectral measurements of the microbial mats near the water's edge, the perceived water color from recorded photos near the center of the pool, thermal images of the pool, simulated spectra for the center of the pool using the optical model from Section 2, and simulated images of the pool colors.

It is important to note that the spectra were measured in terms of spectral reflectance, calibrated using a Spectralon reflectance target illuminated by sunlight. Therefore, rather than a measurement of water reflectance, each measurement should be considered to be a ratio of upwelling spectral irradiance from the water or microbial mat [E from Eq. (1)] to the downwelling solar spectral irradiance (E_{sun}). The upwelling irradiance includes reflected light, but also the backward-scattered light contributions from the water. Appendix A provides data for three

(a)

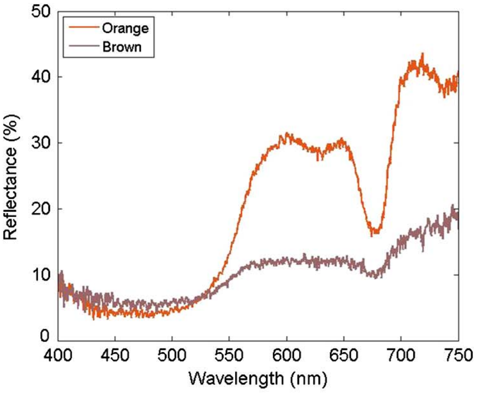

(b)

Fig. 4. (a) Photograph of the orange and brown microbial mats found in the outflows of Grand Prismatic Spring and (b) associated spectral measurements. The "o" and "b" in the photograph mark the locations of the orange and brown spectra.

additional pools surveyed during our experiments, but not discussed in the body of this paper.

A. Grand Prismatic Spring (Midway Geyser Basin)

Grand Prismatic Spring (area = 76 m × 85 m, depth = 50 m, pH 8.3 to 8.1, temperature 63°C to 74°C) is the largest hot spring in YNP and the third largest in the world [3]. This spring, shown in Fig. 3(a), is a good example of the rainbow of colors that can be observed in such hot pools. The mildly basic water flowing from the spring feeds the diversity of microbial mats surrounding and in the pool. The shallow outflows, typically less than 10 cm deep and lower in temperature (minimum of 23.3°C [3]), host dense microbial mats that give them their characteristic orange, red, or brown color. These outflows can be seen as the tendrils extending away from the pool.

Figure 3(b) shows a thermal image of Grand Prismatic Spring using 8 stitched images from a FLIR Photon 640 IR camera (colors in the online version indicate low temperatures in blue and hot temperatures in red). This image shows the variation of water skin temperature across the pool (high absorption prevents measuring water below the surface), with the water cooling while flowing outward from the center. This change in temperature is also associated with a change in the colors of the microbial mats seen in Fig. 3(a). The thermal measurements should be considered only an estimate of the water skin temperature because of incomplete correction for atmospheric effects. The images were collected at an oblique angle near 80°, where there is significant reflection of the cold sky. The image in Fig. 3(b) has been corrected for the reflected sky emission at an assumed near-horizon sky brightness temperature of −20°C with average water emissivity of 0.75, but there has been no correction for atmospheric absorption and emission in the approximately 230 m path between the observation point and the pool.

Figure 4(a) is a close-up photograph of the orange and brown outflow from Grand Prismatic Spring, and Fig. 4(b) is a pair of spectra measured at the locations indicated in Fig. 4(a) for the orange ("o") and brown ("b") mats. The spectra were recorded by collecting light reflected from the mat with an optical fiber attached to a long stick held approximately 1 m above the outflow. The acceptance angle of the spectrometer's input fiber was reduced with a baffle to create a 2.5° half-angle field of view, which sampled a 8.7-cm diameter water area. The measured spectra nicely explain the orange color, with predominantly yellow and red reflection components and strongly suppressed green reflection. The increase below 450 nm is not important for visual perception since the sensitivity of human vision and visible camera detectors is already quite low at those wavelengths.

Although we cannot determine for certain if the bottom is covered with a uniform mat, the water temperature range suggests that mats could grow throughout this pool (except possibly near the vent where temperatures up to 86°C have been reported [3]). The pool edge—which we could see but could not access easily with our spectrometer—looked quite yellow, with brown and orange mats only apparent in the outflow with lower temperatures (recall that Table 1 relates brown and orange to lower temperatures). Therefore, our model assumed that the pool bottom was uniformly covered with a yellow mat. Since we could not measure a yellow mat at Grand Prismatic Spring, we used a similar measurement from the outflow of Sapphire Pool (Fig. 14). To model the visible color we applied the procedure described

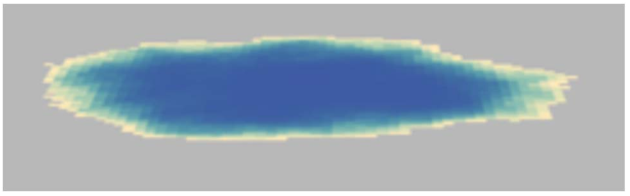

Fig. 5. Simulation of Grand Prismatic Spring for a viewing angle of 80° for comparison with Fig. 3(a). The simple model nicely reproduces the observed yellow-to-turqoise-green and then blue color gradient from the edge to the center of the pool.

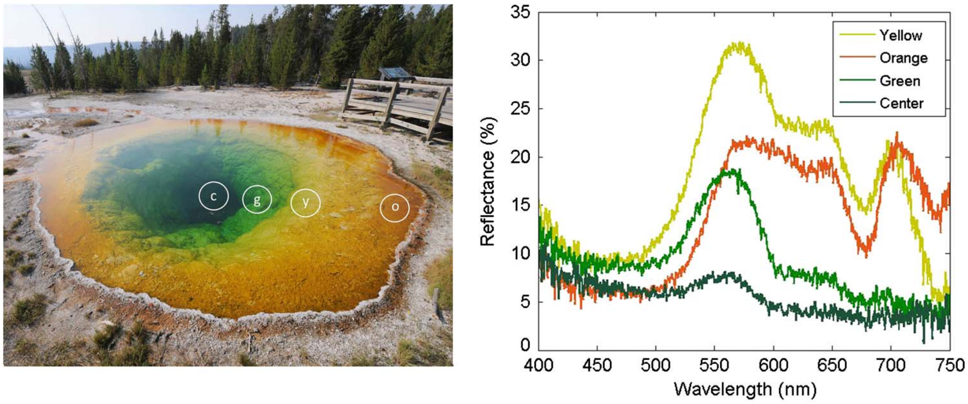

(a) (b)

Fig. 6. (a) Photograph of Morning Glory Pool (Upper Geyser Basin) and (b) spectra recorded at the positions indicated in the photo ("o" = orange, "y" = yellow, "g" = green, "c" = center).

in Section 2 for a conical pool of 50 m depth. The result is shown in Fig. 5 for an observation angle of 80° for comparison with Fig. 3(a) (the simulation was done for the full pool depth and then a perspective transform was applied to match the perspective of the photograph). The pool center—though presumably covered by the yellow mat—appears deep blue, indicating that the pool is deep enough that backward-scattered sunlight from the water is the dominant component of upwelling light. However, for the shallow regions with outflows near the pool edge, the dominant component is sunlight reflected from the mats, yielding the yellowish edge. Our simple model nicely reproduces the observed blue colors of the pool as well as the colorful edge effects. The observed color gradient from yellow to green and then blue is nicely reproduced from the edge to the center of the pool. The center region of Fig. 3(a) is a lighter blue because of steam, which was not included in the simulation.

B. Morning Glory Pool (Upper Geyser Basin)

From early 1880 through the 1940 s, Morning Glory Pool (area = 7 m × 8 m, depth = 7 m, pH 5.8, temperature = 69.8°C) resembled the morning glory flower and was deep blue at the center [3]. Early surveys of the park measured the temperature of this pool to be 78°C [7]. However, as a result of coins, trash, and rocks thrown into the pool over time, the vent has become partially blocked, leading to a lower temperature and altered color pattern. Our photographs and spectra collected in August 2012 show that the pool was a combination of orange, yellow, and green, presumably because microbial mats, formerly only living on the periphery, now thrive in the center of the pool as a result of the decreased temperature [3,4].

Figure 6(a) is a photograph of Morning Glory Pool, with its colorful mats showing clearly through the shallow water near the pool edge, and Fig. 6(b) shows four spectra of the yellow, orange, green, and center region (locations indicated by circles in Fig. 6(a). The spectra were recorded in the manner discussed for Fig. 4(b) and again nicely explain the observed colors. According to the pool temperature of 69.8°C, we used the yellow spectrum of Fig. 6(b) for the entire pool bottom and applied the previously described modeling procedure for a maximum depth of 7 m. A simulated pool image is shown in Fig. 7 for comparison with Fig. 6(a). The pool center exhibits blue-green color, indicating that the pool is just deep enough for backward scattering to become significant in the observed upwelling light. However, for the shallow outflows near the border of the pool, the reflection from the mats dominates, yielding the colorful edges. The simple model nicely reproduces the observed colors of the pool, including the edge effects.

Before the vents were partially plugged, Morning Glory Pool was reported to be much warmer, near 78°C, and was reported to be primarily blue in color. To model such a pool, the yellow microbial mat spectrum was replaced with the spectrum from gray rock near the pool. This yielded a simulated pool image

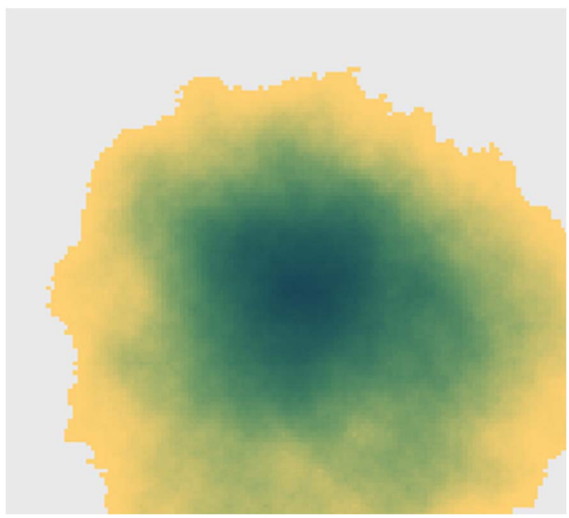

Fig. 7. Simulated color image for Morning Glory Pool using 7 m depth with a single-species yellow cyanobacteria mat whose spectrum was measured in shallow waters near the pool edge.

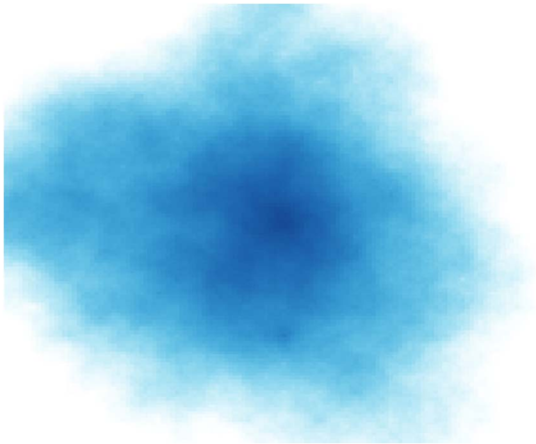

Fig. 8. Simulated color image for a historic Morning Glory Pool that had higher water temperature and no microbial mat.

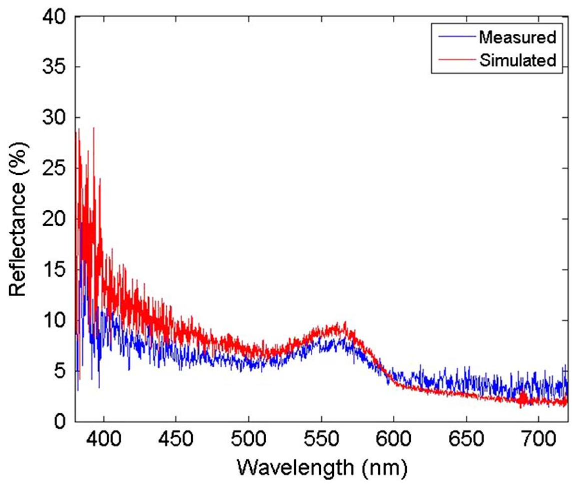

Fig. 9. Simulated (upper red) and measured (lower blue) reflection spectra for the center of Morning Glory Pool. The comparison shows good agreement, with a mean reflectance difference of 1.8% and an RMS reflectance difference of 3.4%.

with only a deep blue color (Fig. 8), which agrees nicely with historical descriptions.

The simulated spectrum for the pool center was compared with a measured spectrum [lower curve in Fig. 6(b)] that had been normalized with a Spectralon reflectance reference and displayed in terms of reflectance (or a ratio of upwelling to downwelling irradiance reflected from a Lambertian target). To convert the simulated spectral irradiance $E(\lambda)$ obtained in step 6 of the modeling procedure into such a ratio, it was divided by the incident solar irradiance $E_{\text{sun}}(\lambda)$. This ratio multiplied by 100 is referred to as the simulated reflectance. In Fig. 9 the simulated (upper red) and measured (lower blue) reflectance spectra for the center of Morning Glory Pool show good agreement, with a mean reflectance difference of 1.8% and rms difference of 3.4% reflectance. The simulated reflectance is higher than the observed spectrum by 3.5% at 400 nm, lower by 1.5% at 700 nm, and equal to the measured spectrum at 595 nm. These differences may result from some combination of sky whitening by wildfire smoke, the presence of biological material or dissolved minerals in the water that was modeled as pure, or shading due to pool geometry.

C. Sapphire Pool (Biscuit Basin, Part of the Upper Geyser Basin Group)

Sapphire Pool is a remarkably clear pool, with a deep blue color resembling a sapphire gem. Today this pool is one of the hottest in the park, with the mildly basic water (pH 8.06 [3]) typically just under the 93° C boiling temperature of water for this elevation (~2225 m). It has been observed to actually boil occasionally [3,4]. With such high temperatures, this pool completely lacks a microbial mat. This, combined with the whitish-gray rock bottom of the pool, leads to nearly all the color arising from absorption and backward scattering in the water. Figure 10 shows a photograph of Sapphire Pool and spectra measured for the deep blue water near the center of the pool and for the grayish-white rock at the side of the pool.

Figure 11 shows a simulated image that assumed 90°C water in a 9 m × 5 m cone-shaped pool of 20 m depth [3]. This simulation omitted a microbial mat and instead used the dry soil spectrum from Fig. 10(b) to model the bottom reflectance. This

(a)

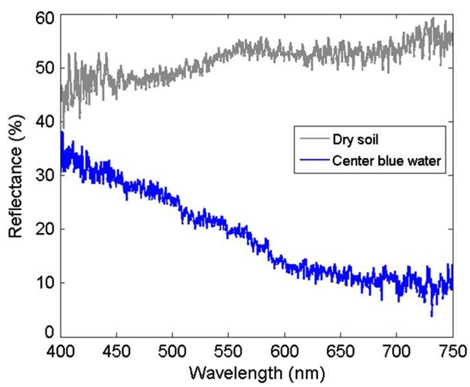

(b)

Fig. 10. (a) Photograph and (b) spectrum measured near the dark center of Sapphire Pool.

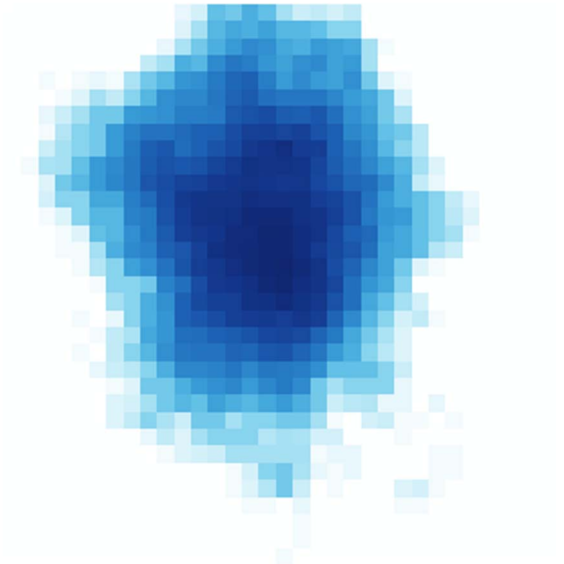

Fig. 11. Simulated color image for Sapphire Pool with no microbial mat.

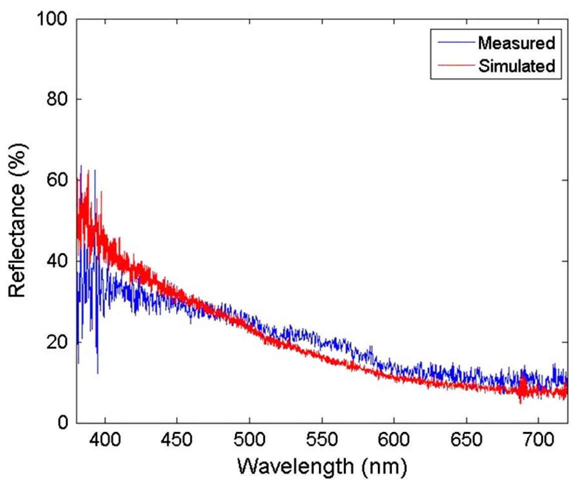

Fig. 12. Simulated (upper red at short wavelengths) and measured (lower blue at short wavelengths) reflection spectra for the center of Sapphire Pool. The mean reflectance difference is 1.4% and the RMS difference is 6.5%.

simulation easily reproduces the deep-blue sapphire color that leads to the name of this pool. Comparing Fig. 11 to the historic Morning Glory Pool simulation in Fig. 8 reveals that the larger depth of Sapphire Pool leads to a deeper blue color, as expected. Note also that the presence of white steam reduces the color saturation, but not the hue.

Figure 12 shows the measured and simulated spectra for Sapphire Pool, which agree within a mean reflectance difference of 1.4% and an RMS difference of 6.5%. Both spectra show increased upwelling light at blue wavelengths, but again the simulation has slightly more blue content than the measurement. The simulated reflectance is 7% higher at 400 nm, 2% lower at 700 nm, and equal to the measured spectrum at 470 nm. Scattering by suspended particles would be most significant at shorter wavelengths where most of our error is observed. Since this water is not truly sterile, it is likely that the assumption of pure water is not accurate and an improved model would include dissolved minerals or biological matter. This also could be caused partially by steam, which would reduce the blue light and increase the red light.

Observations in the Shallow Outflows of Sapphire Pool

In shallow waters, such as the outflows of Sapphire Pool, there is a color change from yellow-green to brown, and then to orange, which is directly correlated to temperature-related microbial mats. This can be seen in visible and thermal images of the Sapphire Pool outflow (Fig. 13). Figure 13 shows the close relationship between the observed colors (a) and the temperature of the outflow (b). Figure 14 shows spectra measured at each location marked in Fig. 13(a), along with a temperature profile across the water from the thermal image. The likely effect of UV irradiance on microbial mat color was illustrated by the transition of the yellow–green mat to a dark green color when the water passed under the boardwalk. Note that this shallow water has no significant contribution of absorption and scattering.

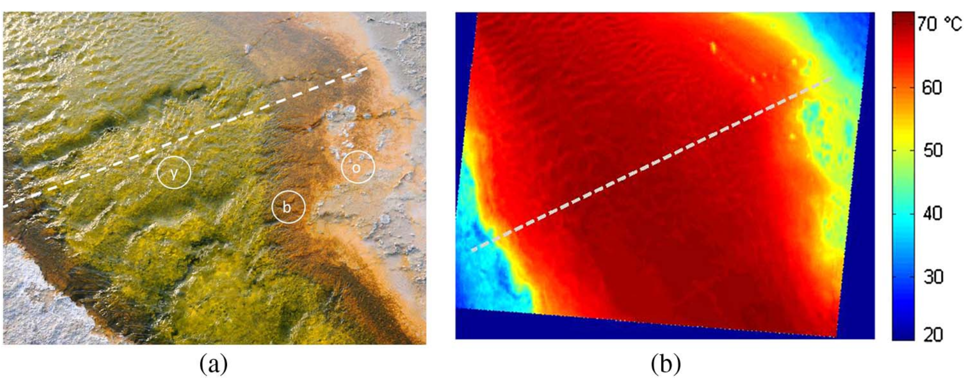

Fig. 13. (a) Photograph and (b) thermal IR image of a shallow Sapphire Pool outflow (Biscuit Basin). The color change from orange (o) and brown (b) at the edges to yellow–green (y) at the center corresponds closely to the respective temperatures. The dashed gray line is the location of the temperature profile shown in Fig. 14(b).

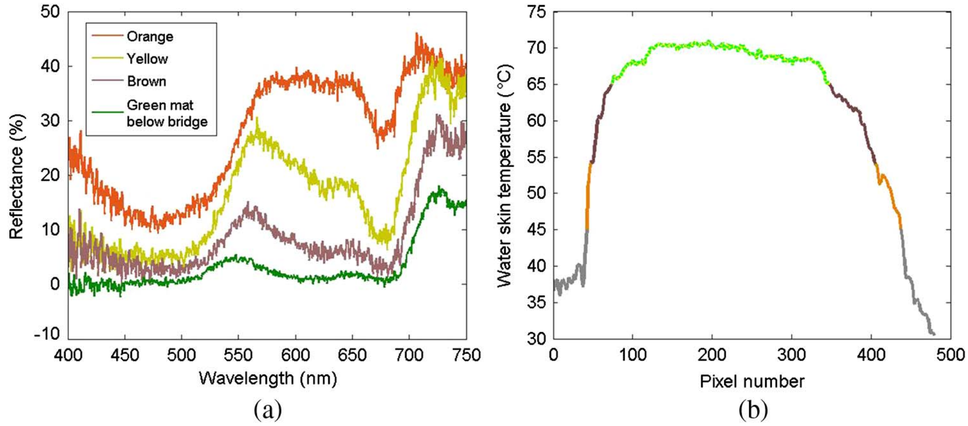

Fig. 14. (a) Spectra measured from the Sapphire Pool outflow in Biscuit Basin at locations marked on Fig. 13(a); (b) water skin temperature profile across the shallow outflow water at the location marked in Fig. 13(b). The profile is plotted such that the color of the line matches the color of the microbial mat expected at each range of water temperatures. The outer edges of the temperature-profile line are gray, representing bare rock.

4. Conclusion

The brilliant and varied colors of various hot springs and pools in Yellowstone National Park (YNP) can be reproduced using a relatively simple one-dimensional radiative transfer model that includes the optical absorption and scattering of water, incident solar and diffuse skylight illumination, and spectral reflectance of the microbial mats measured near the pools. This model produced simulations that were visually similar to photographs of the pools.

Color changes in shallow water were shown to relate to changes in the microbial mats and water temperature. In these cases, the observed colors were most directly related to the spectral properties of microbial mats that change with water temperature. However, color changes in deeper water from yellow to green and then blue were not associated with temperature gradients, but were instead driven by absorption and scattering in the water. Examples of this kind of color transition were shown for both Morning Glory Pool and Grand Prismatic Spring. In Morning Glory Pool, a yellow microbial mat beneath moderately deep water appears green, while the much deeper water of Grand Prismatic Spring appears blue because of wavelength-dependent scattering in the water, which is weighted heavily toward the blue. In such deep pools, scattering from the pool bottom can be neglected.

It is suggested throughout the literature that lower levels of UV-irradiance can lead to an increase in chlorophyll and decrease in carotenoids and phycobiliproteins. This would lead to a color shift from yellow to green in the microbial mat. It has been suggested that this could be the cause of the yellow-to-green transition observed in many pools. As the water depth increases, the UV irradiance decreases and could change the microbial mat. However, the simulations presented here show that wavelength-selective optical transmission in water is sufficient to reproduce this color change. Thus, a change in the microbial mats is not required to describe the yellow-to-green transition observed with increasing water depth. However, chlorophyll-related green color is occasionally also observable in very shallow outflows, typically in spots where UV radiation from the Sun is blocked. The most prominent example in our study was below a boardwalk near Sapphire Pool which resulted in a very deep green mat.

The model also produced pool-center spectra that agreed with measured spectra to within 1.4% reflectance for Morning Glory Pool and 1.5% for Sapphire Pool. Our simulated spectra are usually greater than the observed data at short wavelengths. This difference could result from one or more of the following factors: smoke particles in the atmosphere, biological material or dissolved minerals in the water, or shading by the pool geometry. There was also a notable amount of smoke in the air on both measurement days, which may have led to somewhat blue-depleted skylight reflecting from the water surfaces. Suspended particles in the water also could have a significant contribution at shorter wavelengths where most of our error is observed. Since the water is not truly sterile, it is likely that the assumption of pure water is not accurate and the presence of dissolved minerals or biological matter had a significant impact at shorter wavelengths, which is not accounted for in the model.

Finally, we note that the good agreement between simulated and observed pool color for known temperatures and pool depths might suggest a way to estimate unknown depths at the center of the pools whose temperatures are known. This argument could also be turned around: once pool depth is known, observed color changes might be useful to detect microbial mat changes that could be caused by temperature changes in the pool.

Appendix A

Here, we provide a brief description of three other pools, along with measured spectra and photographs. For each of these pools, we provide a summary of

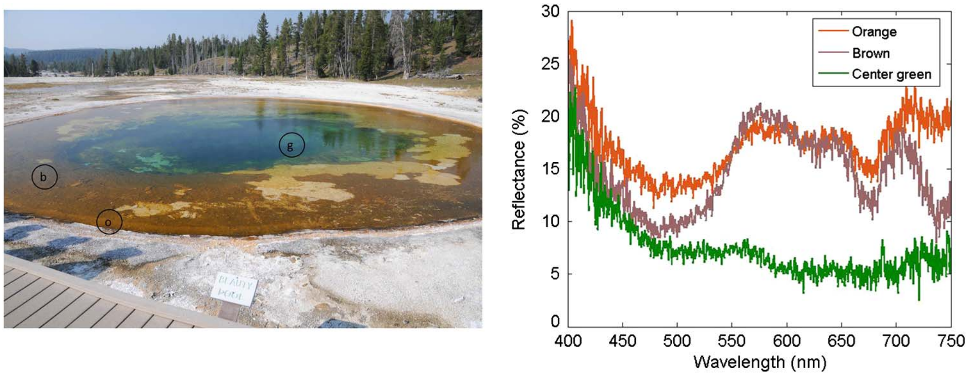

(a) (b)

Fig. 15. Beauty Pool (Upper Geyser Basin): (a) photograph and (b) spectra measured at locations indicated in (a).

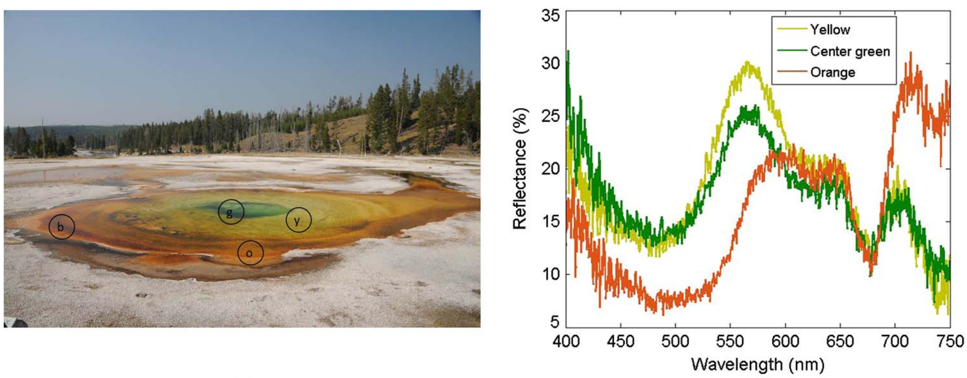

(a) (b)

Fig. 16. Chromatic Pool (Upper Geyser Basin): (a) photograph and (b) spectra measured at locations indicated on the image.

properties, a color photo, and spectra of colored regions recorded at the center or at the sides of each.

Beauty Pool (Upper Geyser Basin)

Beauty Pool (diameter = 18.3 m, depth = 7.6 m [3]) is a colorful pool whose temperature (73°C to 79°C) favors yellow bacteria mats on the deep pool rocks. In shallow regions, lower temperatures allow for brown and orange mats. Therefore, this rather deep pool again follows the scheme of having a deep blue center and colorful edges with orange or brown mats. This pool appears to have some regions where the mats have broken off or been damaged (this was unique within the pools we observed). Its plumbing system is connected to the neighboring Chromatic Spring (see next section). Figure 15 shows a photograph and measured spectra.

Chromatic Spring (Upper Geyser Basin)

Chromatic Spring (diameter = 18 m, temperature = 73°C to 79°C) has large areas that are quite shallow, and it therefore exhibits very colorful mats. Its center seems also to be rather shallow, since the center appears green rather than blue. Therefore, the maximum depth along the sight path should be less than about 5 m. Chromatic and Beauty Pool have an interconnected plumbing system. When one pool begins to overflow, the water level in the other drops, and the temperature of the shallower pool drops by up to 3.5°C [3]. The time interval between shifts ranges from weeks to years [4]. During our observations, the flow was from Chromatic pool, which was observed to be the most colorful. Thus, the lack of yellow mats at the published temperature of Beauty Pool is likely a result of reduced water temperature at the time of observation. Figure 16 shows a photograph of Chromatic Spring and spectra measured at the orange, yellow, and green regions indicated on the photograph.

Belgian Pool (Upper Geyser Basin)

In our images of Belgian Pool, the angle of observation only allowed small distances within water, so its center appeared clear with only a light blue hue. The center region has no mats, which suggests that photosynthesis has stopped, suggesting either chemistry changes or temperatures above those quoted in the literature (temperature = 66.4°C, 74°C at vent [4]; pH = 8.99). Figure 17 shows a photograph of Belgian Pool and spectra measured at the clear light-blue water and the brown mat.

Portions of this research were performed with funding from the U.S. National Science Foundation through Award ARC-1108427.

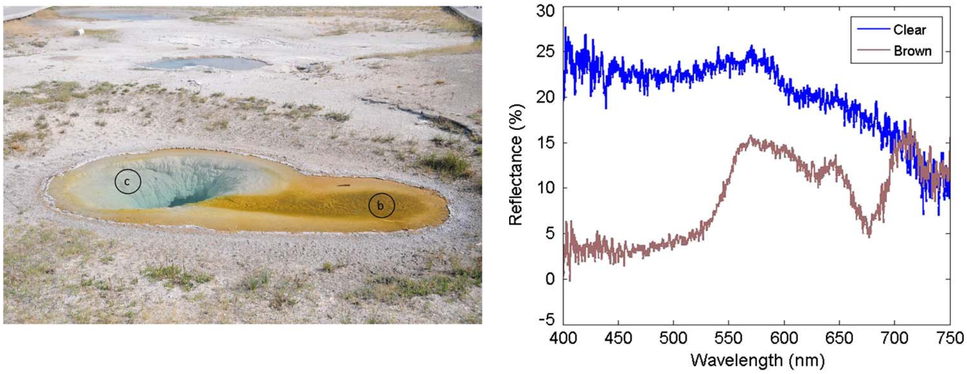

(a) (b)

Fig. 17. Belgian Pool (Upper Geyser Basin): (a) photograph and (b) spectra measured at locations indicated on the image.

References

1. M. Brody and W. Tomkiewicz, "Park visitors' understandings, values and beliefs related to their experience at Midway Geyser Basin, Yellowstone National Park, USA," Int. J. Sci. Ed. **24**, 1119–1141 (2002).
2. F. V. Hayden, *Preliminary Report of the United States Geological Survey of Montana and Portions of Adjacent Territories; Being a Annual Report Of Progress* (U.S. Government Printing Office, 1872).
3. C. Schreier, *A Field Guide to Yellowstone's Geysers, Hot Springs, and Fumaroles* (Homestead, 1992).
4. Yellowstone National Park Research Coordination Network, http://www.rcn.montana.edu/.
5. D. M. Ward, M. J. Ferris, S. C. Nold, and M. M. Bateson, "A natural view of microbial biodiversity within hot spring cyanobacterial mat communities," Microbiol. Mol. Biol. Rev. **62**, 1353–1370 (1998).
6. T. D. Brock, "Life at high temperatures," Science **230**, 132–138 (1985).
7. J. J. Copeland, "Yellowstone thermal myxophyceae," Ann. N.Y. Acad. Sci. **36**, 4–223 (1936).
8. W. H. Weed, "The vegetation of hot springs," Am. Nat. **23**, 394–400 (1889).
9. K. B. De León, R. Gerlach, B. M. Peyton, and M. W. Fields, "Archaeal and bacterial communities in three alkaline hot springs in Heart Lake Geyser Basin, Yellowstone National Park," Front. Microbiol. **4**, 1–10 (2013).
10. R. W. Renaut and B. Jones, "Microbial precipitates around continental hot springs and geysers," in *Microbial Sediments*, R. Riding and S. Awramik, eds. (Springer, 2000), pp. 187–195.
11. R. T. Papke, N. B. Ramsing, M. M. Bateson, and D. M. Ward, "Geographical isolation in hot spring cyanobacteria," Environ. Microbiol. **5**, 650–659, 2003.
12. S. Ohsawa, T. Kawamura, N. Takamatsu, and Y. Yusa, "Rayleigh scattering by aqueous colloidal silica as a cause for the blue color of hydrothermal water," J. Volcanol. Geotherm. Res. **113**, 49–60 (2002).
13. A. Cox, E. L. Shock, and J. R. Havig, "The transition to microbial photosynthesis in hot spring ecosystems," Chem. Geol. **280**, 344–351 (2011).
14. T. Nakagawa and M. Fukui, "Phylogenetic characterization of microbial mats and streamers from a Japanese alkaline hot spring with a thermal gradient," J. Gen Appl. Microbiol. **48**, 211–222 (2002).
15. R. W. Castenholz, J. Bauld, and B. B. Jørgenson, "Anoxygenic microbial mat of hot springs: thermophilic chlorobium sp.," FEMS Microbiol. Lett. **74**, 325–336 (1990).
16. C. T. Brues, "Animal life in hot springs," Q. Rev. Biol. **2**, 181–203 (1927).
17. A. H. Segrer, S. Burggraf, G. Fiala, G. Huber, R. Huber, U. Pley, and K. O. Stetter, "Life in hot springs and hydrothermal vents," Orig. Life Evol. Biosph. **23**, 77–90 (1993).
18. C. R. Lehr, S. D. Frank, T. B. Norris, S. D'Imperio, A. V. Kalinin, J. A. Toplin, R. W. Castenholz, and T. R. McDermott, "Cyandia (Cyanidiales) population diversity and dynamics in an acid-sulfate-chloride spring in Yellowstone National Park," J. Phycol. **43**, 3–14 (2007).
19. R. C. Smith and K. S. Baker, "Optical properties of the clearest natural waters," Appl. Opt. **20**, 177–184 (1981).
20. H. Buiteveld, J. H. M. Hakvoort, and M. Donze, "The optical properties of pure water," Proc. SPIE **2258**, 174–183 (1994).
21. G. N. Plass, T. J. Humphreys, and G. W. Kattawar, "Color of the ocean," Appl. Opt. **17**, 1432–1446 (1978).
22. A. Morel, B. Gentili, H. Claustre, M. Babin, A. Bricaud, J. Ras, and F. Tieche, "Optical properties of the "clearest" natural waters," Limnol. Oceanogr. **52**, 217–229 (2007).
23. C. Giardino, A. Oggioni, M. Bresciani, and H. Yan, "Remote sensing of suspended particulate matter in Himalayan lakes: a case study of alpine lakes in the Mount Everest region," Mt. Res. Dev. **30**, 157–168 (2010).
24. A. Albert and C. D. Mobley, "An analytical model for subsurface irradiance and remote sensing reflectance in deep and shallow case-2 waters," Opt. Express **11**, 2873–2890 (2003).
25. Y. Oyama and A. Shibahara, "Simulation of water colors in a shallow acidified lake, Lake Onneto, Japan, using colorimetric analysis and bio-optical modeling," Limnology **10**, 47–56 (2009).
26. D. Mobley, "Optical properties of water," in *Handbook of Optics*, M. Bass, E. W. Van Stryland, D. R. Williams, and W. L. Wolfe, eds. 2nd ed., Vol. **I** (McGraw-Hill, 1995), Chap. 43.
27. A. Berk, G. P. Anderson, P. K. Acharya, L. S. Bernstein, L. Muratov, J. Lee, M. Fox, S. M. Adler-Golden, J. H. Chetwynd, M. L. Hoke, R. B. Lockwood, J. A. Gardner, T. W. Cooley, C. C. Borel, and P. E. Lewis, "MODTRAN 5: a reformulated atmospheric band model with auxiliary species and practical multiple scattering options: update," Proc. SPIE **5806**, 662–667 (2005).
28. G. P. Anderson, S. A. Clough, F. X. Kneizys, J. H. Chetwynd, and E. P. Shettle, "AFGL atmospheric constituent profiles (0–120 km)," AFGL-TR-86-0110, Environmental Research Papers (U.S. A.F. Geophysical Laboratory), 954 (1986), available from National Technical Information Service, Alexandria, Virginia (www.ntis.gov) (also available at http://oai.dtic.mil/oai/oai?verb=getRecord&metadataPrefix=html&identifier=ADA175173).
29. SNOTEL Data: Station 384 Canyon, Wyoming, United States Department of Agriculture, Natural Resources Conservation Service, http://www.wcc.nrcs.usda.gov/nwcc/site?sitenum=384 (2014).
30. P. Tans, NOAA/ESRL (www.esrl.noaa.gov/gmd/ccgg/trends/) and R. Keeling, Scripps Institution of Oceanography (scrippsco2.ucsd.edu/).
31. A. Fournier, D. Fussell, and L. Carpenter, "Computer rendering of stochastic models," Commun. ACM **25**, 371–384 (1982).